

Physical properties of $K_xNi_{2-y}Se_2$ single crystals

Hechang Lei,¹ Kefeng Wang,¹ Hyejin Ryu,^{1,2} D. Graf,³ J. B. Warren,⁴ and C. Petrovic^{1,2}

¹*Condensed Matter Physics and Materials Science Department,
Brookhaven National Laboratory, Upton, NY 11973 USA*

²*Department of Physics and Astronomy, State University of New York, Stony Brook, NY 11794-3800, USA*

³*NHMFL/Physics, Florida State University, Tallahassee, Florida 32310, USA*

⁴*Instrumentation Division, Brookhaven National Laboratory, Upton, New York 11973, USA*

(Dated: March 3, 2018)

We have synthesized $K_{0.95(1)}Ni_{1.86(2)}Se_2$ single crystals. The single crystals contain K and Ni deficiencies not observed in KNi_2Se_2 polycrystals. Unlike KNi_2Se_2 polycrystals, the superconductivity is absent in single crystals. The detailed physical property study indicates that the $K_{0.95}Ni_{1.86}Se_2$ single crystals exhibit Fermi liquid behavior with heavy-fermion-like characteristics. Transition from the high temperature local charge density wave state to heavy fermion state below $T \sim 30$ K results in an enhancement of electron-like carrier density whereas magnetic susceptibility shows little anisotropy and suggests presence of both itinerant and localized Ni orbitals.

PACS numbers: 74.70.Xa, 74.70.Tx, 71.27.+a, 71.45.Lr

I. INTRODUCTION

Even before the discovery of superconducting $T_c = 26$ K in $LaFeAsO_{1-x}F_x$,¹ some nickel pnictide materials (such as $LaONiP$)² have already been found to become superconducting (SC) at low temperature. Examples of nickel pnictide superconductors include also $LaONiAs$, $LaO_{1-x}NiBi$, $BaNi_2P_2$ and $SrNi_2P_2$.³⁻⁶ However, all nickel pnictide SCs have much lower T_c (< 5 K) when compared to iron pnictide SCs of which T_c 's are mostly well above 5 K.⁷ The possible reason leading to this difference could be due to the different superconducting mechanisms or to the different values of materials parameters relevant for superconductivity which are not optimized for the nickel pnictides even if the pairing mechanism would be identical.⁷

On the other hand, iron chalcogenide SCs have also been discovered, including $FeCh$ ($Ch = S, Se, Te$),⁸⁻¹⁰ and $A_xFe_{2-y}Se_2$ ($A = K, Rb, Cs, Tl/K$ and Tl/Rb).¹¹⁻¹⁶ In contrast to iron chalcogenide SCs, however, corresponding nickel chalcogenide SCs are still missing. $NiSe$ has $NiAs$ type structure with space group $P63/mmc$ and this structure is isostructural to hexagonal $FeSe$ (high temperature phase). $NiSe$ is a non-superconducting metal with ferromagnetic fluctuations.¹⁷ Similarly, $TlNi_2Se_2$ is a Pauli paramagnet without superconducting transition down to 2 K.¹⁸ However, very recently, it was reported that KNi_2Se_2 polycrystals are superconducting with $T_c = 0.80(1)$ K.¹⁹ Moreover, KNi_2Se_2 single crystals feature a heavy-fermion-like state with an increased carrier mobility and enhanced effective electronic band mass below about 40 K. This state should emerge from the local charge density wave (CDW) state which persists up to 300 K.

A study of single crystals is necessary in order to elucidate the anisotropy in intrinsic physical properties of KNi_2Se_2 and eliminate the influence of grain boundaries and ferromagnetic Ni impurities. Hence in this work we report the physical properties of $K_{0.95(1)}Ni_{1.86(2)}Se_{2.00(1)}$

single crystals. Unexpectedly, we found no evidence for superconducting transition down to 0.3 K in resistivity measurement. Magnetic, Hall, thermodynamic and thermal measurements suggest that the heavy-fermion-like properties of $K_xNi_{2-y}Se_2$ arise from dominant electron-like carriers. The Fermi surface reconstruction with increased electron-like carrier concentration at $T \sim 30$ K marks the crossover from local CDW state at high temperatures to the low temperature heavy-fermion-like state.

II. EXPERIMENT

Single crystals of KNi_2Se_2 were grown by self-flux method similar to $K_xFe_{2-y}Se_2$ ²⁰ with nominal composition $K:Ni:Se = 1:2:2$. Briefly, prereacted $NiSe$ and K pieces were added into the alumina crucible with partial pressure of argon gas. The quartz tubes were heated to 1030 °C, kept at this temperature for 3 hours, then cooled to 730 °C with 6 °C/h. The platelike dark pink colored single crystals with typical size $5 \times 5 \times 2$ mm³ can be grown. X-ray diffraction (XRD) spectra were taken with $Cu K_\alpha$ radiation ($\lambda = 1.5418$ Å) using a Rigaku Miniflex X-ray machine. The lattice parameters were obtained by fitting the XRD spectra using the Rietica software.²¹ The elemental analysis was performed using an energy-dispersive x-ray spectroscopy (EDX) in a JEOL JSM-6500 scanning electron microscope. Electrical and thermal transport, heat capacity, and magnetization measurements were carried out in Quantum Design PPMS-9 and MPMS-XL5. The in-plane resistivity $\rho_{ab}(T)$ was measured using a four-probe configuration on cleaved rectangularly shaped single crystals with current flowing in the ab -plane of tetragonal structure. Thin Pt wires were attached to electrical contacts made of silver paste. Thermal transport properties were measured in Quantum Design PPMS-9 from 2 to 350 K using a one-heater two-thermometer method. The relative error was

$\frac{\Delta\kappa}{\kappa} \sim 5\%$ and $\frac{\Delta S}{S} \sim 5\%$ based on Ni standard measured under identical conditions.

III. RESULTS AND DISCUSSION

As shown in Fig. 1(a), powder XRD pattern of KNi_2Se_2 can be fitted very well using the $I4/mmm$ space group. The determined lattice parameters are $a = 0.3899(2)$ nm and $c = 1.3473(2)$ nm. The value for a axis is somewhat smaller whereas the c axis lattice parameter is larger when compared to polycrystalline samples with full occupancies of K and Ni ($a = 0.39098(8)$ nm and $c = 1.34142(5)$ nm).²² This is in agreement with previous study which indicated that the deviation from full occupancy can increase the c lattice parameter with only minor effect on a lattice parameter.²² On the other hand, both a and c lattice parameters are smaller than those in $\text{K}_x\text{Fe}_{2-y}\text{Se}_2$ ($a = 0.39109$ nm and $c = 1.4075$ nm).²⁰ It could be due to the smaller ionic radius of Ni^{2+} (55 pm) than Fe^{2+} (63 pm) with four-fold coordination.²³ The antiferromagnetic state in $\text{K}_x\text{Fe}_{2-y}\text{Se}_2$ can increase the lattice parameters further when compared to the non-magnetic state according to the theoretical calculation.²⁴ The crystal structure of KNi_2Se_2 is shown in Fig. 1(b), where antiferrotype-type Ni-Se layers and K cation layers are piled up alternatively along the c axis. XRD pattern of a single crystal (Fig. 1(c)) reveals that the crystal surface is normal to the c axis with the plate-shaped surface parallel to the ab -plane. Fig. 1(d) shows the EDX spectrum of a single crystal of KNi_2Se_2 , confirming the presence of the K, Ni, and Se. The EDX results for several single crystals with multiple measuring points indicate that the crystals are rather homogenous and the determined average atomic ratios are K:Ni:Se = 0.95(1):1.86(2):2.00(1) when fixing Se stoichiometry to be 2. Although the amount of deficiencies is smaller when compared to $\text{K}_x\text{Fe}_{2-y}\text{Se}_2$ crystals,²⁰ it is noticeably higher when compared to polycrystals which feature full occupancies of K, Fe and Se atomic sites.

The temperature dependence of the in-plane resistivity $\rho_{ab}(T)$ of the $\text{K}_{0.95}\text{Ni}_{1.86}\text{Se}_2$ single crystal exhibits metallic behavior with the residual resistivity ratio (RRR) $\rho_{ab}(295 \text{ K})/\rho_{ab}(0.3 \text{ K}) = 5$. The room-temperature value $\rho_{ab}(295 \text{ K})$ ($256 \mu\Omega\text{-cm}$) is slightly smaller than the value in polycrystals ($350 \mu\Omega\text{-cm}$). However, the RRR value is much smaller than that in polycrystals (RRR \sim 175) possibly due to the absence or minimization of Ni impurity in single crystals (high purity Ni can have RRR $>$ 2000).^{19,25} In addition, larger residual resistivity ρ_0 in crystals could come from the increased impurity scattering due to the deficiencies. The most striking feature is the absence of superconducting transition down to 0.3 K in $\text{K}_{0.948}\text{Ni}_{1.86}\text{Se}_2$ single crystals when compared to KNi_2Se_2 polycrystals with $T_c = 0.80(1)$ K.¹⁹ The absence of superconductivity in single crystal could be related to the deficiencies of K and Ni, implying that the superconductivity in KNi_2Se_2 is very sensitive to the

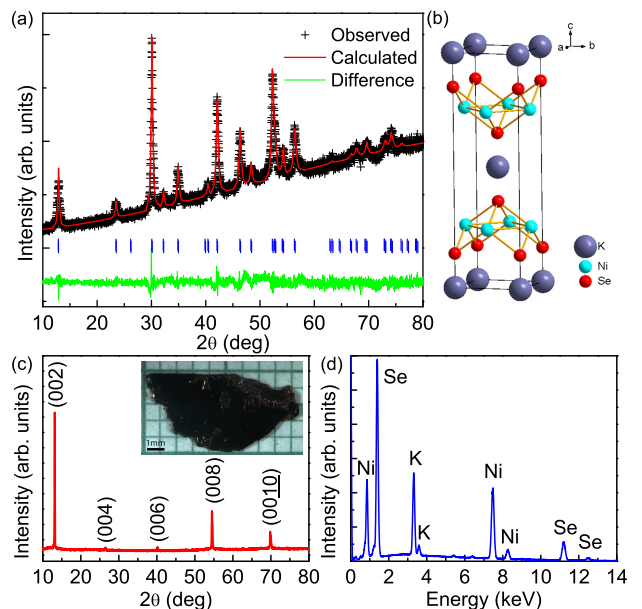


FIG. 1. (a) Powder XRD patterns of $\text{K}_{0.95}\text{Ni}_{1.86}\text{Se}_2$. (b) Crystal structure of KNi_2Se_2 . The big purple, medium cyan and small red balls represent K, Ni, and Se ions. (c) Single crystal XRD of $\text{K}_{0.948}\text{Ni}_{1.86}\text{Se}_2$. The inset shows a photo of typical single crystal of KNi_2Se_2 . The crystals are less air sensitive when compared to $\text{K}_x\text{Fe}_{2-y}\text{Se}_2$ single crystals. (d) The EDX spectrum of a single crystal.

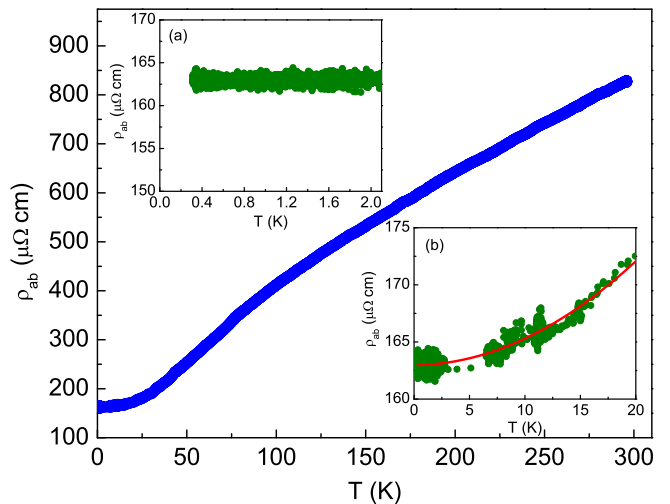


FIG. 2. Temperature dependence of the in-plane resistivity $\rho_{ab}(T)$ of the $\text{K}_{0.95}\text{Ni}_{1.86}\text{Se}_2$ single crystal from 0.3 K to 295 K. The inset (a) shows the enlarged part of $\rho_{ab}(T)$ below 2 K. The inset (b) shows the fitted result from 0.3 K to 20 K using $\rho_{ab}(T) = \rho_0 + AT^n$ where the red line is the fitting curve.

atomic ratio. There is no metal-insulating transition (MIT) in KNi_2Se_2 and the absolute values of resistivity are much smaller when compared to $\text{K}_x\text{Fe}_{2-y}\text{Se}_2$,²⁰ indicating that Ni orbitals in the former are more itinerant when compared to Fe orbitals in the latter material. Surprisingly, as shown in the inset of Fig. 2(b), the $\rho_{ab}(T) \sim T^2$ dependence is observed up to 20 K at tem-

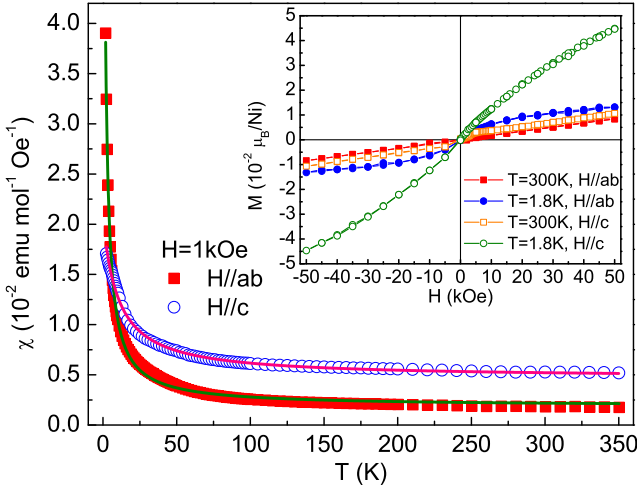


FIG. 3. (a) Temperature dependence of magnetic susceptibility $\chi(T)$ with the applied field $H = 1$ kOe along ab plane and c axis below 300 K. The inset shows the isothermal magnetization hysteresis loops $M(H)$ for $H||ab$ and $H||c$ at 300 K and 1.8 K.

temperatures where other types of scattering (e.g. electron-phonon) are usually active or dominant. From the fit using $\rho_{ab}(T) = \rho_0 + AT^n$, we obtain the residual resistivity $\rho_0 = 50.282(2) \mu\Omega\text{cm}$, the coefficient of the quadratic resistivity term $A = 0.0079(5) \mu\Omega\text{cm}/\text{K}^2$, and $n = 1.96(2)$. It indicates that KNi_2Se_2 enters Fermi-liquid regime at low temperature.

Fig. 3 presents the temperature dependence of magnetic susceptibility $\chi(T)$ of the $\text{K}_{0.95}\text{Ni}_{1.86}\text{Se}_2$ single crystal for $H = 1$ kOe along the ab plane and c axis below 300 K. It can be seen that the $\chi_c(T)$ is larger than the $\chi_{ab}(T)$ at high temperature. The susceptibility can be fitted using Curie-Weiss law $\chi(T) = \chi_0 + C/(T - \theta)$ when a temperature-independent contribution χ_0 is accounted for. Here, χ_0 includes core diamagnetism, Landau diamagnetism, and Pauli paramagnetism, C is Curie constant and θ is the Curie-Weiss temperature (solid lines in Fig. 3). The fitted values for χ_0 are $1.87(5) \times 10^{-3}$ and $4.69(4) \times 10^{-3} \text{ emu mol f.u.}^{-1} \text{ Oe}^{-1}$ for $H||ab$ and $H||c$, which are much larger than the value in literature.²² Because the core diamagnetism is typically on the order of 10^{-6} - $10^{-5} \text{ emu mol}^{-1} \text{ Oe}^{-1}$,²⁶ and $\chi_{\text{Landau}} \approx -1/3\chi_{\text{Pauli}}$, such large χ_0 values strongly imply there is an enhanced Pauli paramagnetism, i.e. the significant pileup of the density of states at the Fermi level due to $\chi_{\text{Pauli}} \approx \mu_B^2 N(E_F)$. On the other hand, the obtained local moment is about 0.463(3) and 0.615(7) μ_B/Ni for $H||ab$ and $H||c$. This is unlikely to be due to impurities such as Ni^{2+} with $S = 1$ because the corresponding molar fraction would be 16.4(1) and 29.7(3) mol% for $H||ab$ and $H||c$, respectively. Such large amount of impurities should have been detected in the XRD pattern, hence the origin of low temperature susceptibility rise should be intrinsic. Contribution of impurity is revealed (Fig. 3 (inset)) in the magnetization loops for both field directions at 300 K and 1.8 K. There is a ferromagnetic

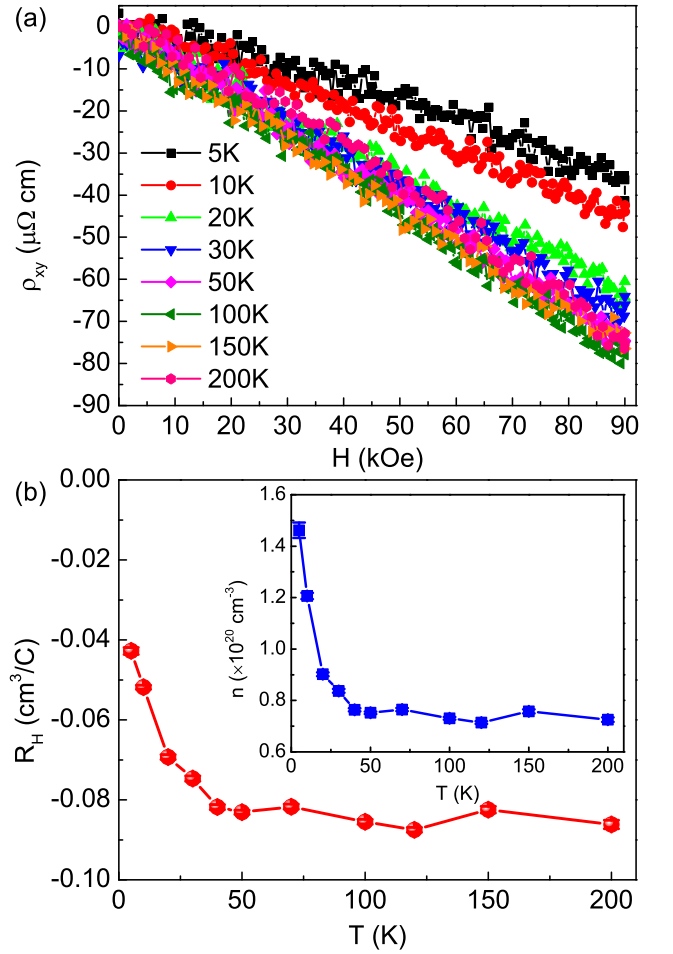


FIG. 4. (a) Field dependence of $\rho_{xy}(H)$ at various temperatures. (b) Temperature dependence of Hall coefficient R_H of $\text{K}_{0.95}\text{Ni}_{1.86}\text{Se}_2$ single crystal. Inset: Temperature dependence of carrier density $n = 1/|eR_H|$ calculated from R_H based on the single band model.

component superposed on the paramagnetic background with very small magnetic moment ($\sim 10^{-2} \mu_B/\text{Ni}$). After subtracting paramagnetic part from the curve for $H||ab$ at 1.8 K, the saturated moment would correspond to ~ 0.2 mol% Ni^{2+} or ~ 1 mol% Ni impurities. The above analysis indicates that Ni orbitals in NiSe_4 tetrahedra are at the boundary of itinerancy and Mott localization with possible orbital dependent correlation strength, similarly to iron orbitals in iron based superconductors.²⁷

As shown in Fig. 4(a), the transverse resistivity $\rho_{xy}(H)$ shows approximately linear relation against the magnetic field and is negative at all measuring temperatures, indicating that the electron-type carrier is dominant. From the linear fitting of $\rho_{xy}(H) - H$ relation, we obtain the Hall coefficients $R_H = \rho_{xy}(H)/H$ at different temperatures, which is shown in Fig. 4(b). It can be seen that the R_H is weakly temperature dependent when $T > 30$ K and then decreases with temperature. In a single band scenario, this change suggest that the carrier density increases at about $T = 30$ K since

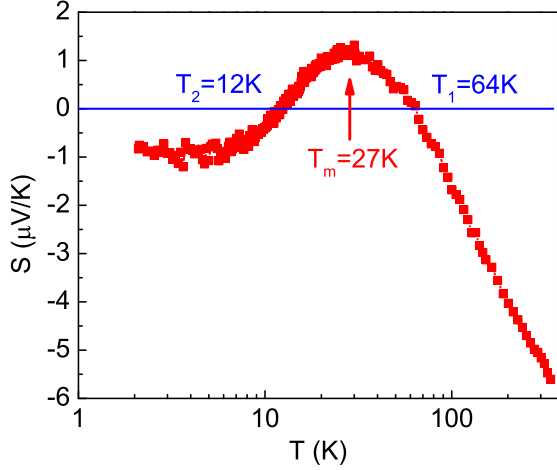


FIG. 5. Temperature dependence of thermoelectric power $S(T)$ for $K_{0.95}Ni_{1.86}Se_2$ single crystal from 2 to 350 K.

$R_H = 1/ne$ (Inset of Fig. 4(b)). This could be related to the crossover from local CDW state to heavy fermion state in KNi_2Se_2 .¹⁹ On the other hand, this can also be ascribed to the multiband effect, which has been observed in classic two band materials such as MgB_2 as well as in iron based material $Nd(O,F)FeAs$.^{28,29} However, the observed temperature dependence is much weaker than that in $Nd(O,F)FeAs$ single crystal, which exhibits significant multiband behavior. It implies the multiband behavior should be weaker in KNi_2Se_2 when compared to iron based superconductors. From obtained R_H , the corresponding carrier density at 300 K is $\sim 4 \times 10^{-3}$ carrier per Ni, increasing up to $\sim 8 \times 10^{-3}$ carrier per Ni. The carrier density is very low, even one order lower than in iron based superconductors, such as $LaFeAsO_{0.89}F_{0.11}$ ($\sim 10^{21} \text{ cm}^{-3}$).³⁰ Moreover, from the measured resistivity at 5 K ($\rho_{ab}(5 \text{ K}) = 4.74 \times 10^{-5} \Omega \text{ cm}$) and derived carrier density at same temperature ($n(5 \text{ K}) = 1.46 \times 10^{20} \text{ cm}^{-3}$), the carrier mobility at 5 K can be roughly estimated using $\sigma = ne\mu$ and is about $905 \text{ cm}^2 \text{ V}^{-1} \text{ S}^{-1}$. It is close to the result derived from magnetoresistance measurement of polycrystals ($1070 \text{ cm}^2 \text{ V}^{-1} \text{ S}^{-1}$), implying that KNi_2Se_2 has high carrier mobility. On the other hand, as discussed below, the electron specific heat is large at low temperature, indicating the increased effective mass. Because μ is proportional to mean scattering time and inversely proportional to the effective mass, the mean scattering time could be rather large at low temperatures.¹⁹

Fig. 5 shows the temperature dependence of thermoelectric power (TEP) $S(T)$ for $K_{0.95}Ni_{1.86}Se_2$ single crystals measured between $T = 2$ and 350 K. At high temperature, the TEP is negative, consistent with dominant negative charge carriers. It is interesting that the value of the TEP decreases with decrease of temperature and then becomes positive at about $T_1 = 64$ K. The sign change implies multiband transport. Even though the Hall coefficient R_H is unchanged in that tempera-

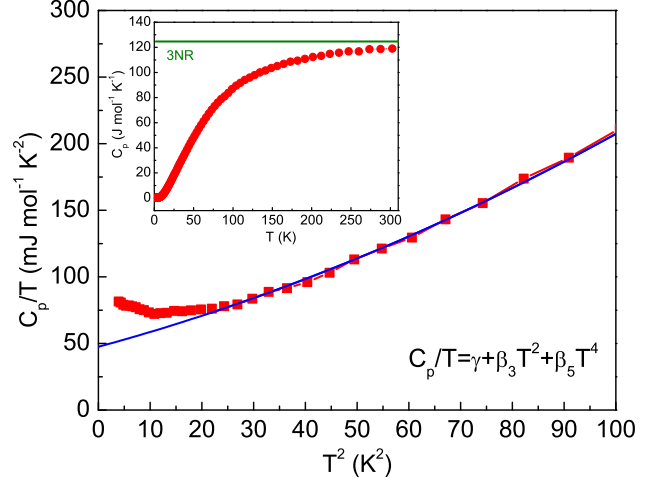


FIG. 6. The relation between C_p/T and T^2 for $K_{0.948}Ni_{1.86}Se_2$ single crystal at low temperature. The solid curve represents the fitting result using the formula $C_p/T = \gamma + \beta_3 T^2 + \beta_5 T^4$. The inset shows the temperature dependence of $C_p(T)$ for whole measuring temperature. The green solid line represents the classical value according to Dulong-Petit law at high temperature.

ture range, the sign of TEP $S(T)$ might change since they have different dependence on carrier density n_e (n_h), mobility μ_e (μ_h), and S_e (S_h) in the two band model ($R_H = \frac{1}{e} \frac{n_h \mu_h^2 - n_e \mu_e^2}{(n_h \mu_h + n_e \mu_e)^2}$, $S = \frac{S_e n_e \mu_e + S_h n_h \mu_h}{n_e \mu_e + n_h \mu_h}$).³¹ With further decreasing temperature, TEP shows a peak at around $T_m = 27$ K and then decreases with temperature. Finally it becomes negative again and the temperature corresponding to the second sign reverse is about $T_2 = 12$ K. The temperature of T_m is very close to the temperature where the change of slope in R_H appears. This suggests that the second sign change of $S(T)$ could be related to the crossover from local CDW state to heavy fermion state where Fermi surface becomes large with increasing carrier density in electron-type bands.

Fig. 6 shows the relation between C_p/T and T^2 for $K_{0.95}Ni_{1.86}Se_2$ single crystal at low temperature. It can be seen that there is an upturn in the specific heat as $T < 3$ K. This upturn could not be related to the superconducting transition or to nuclear Schottky anomaly since it appears at much higher temperatures. This might be an intrinsic effect related to magnetic fluctuations due to the deficiencies of K and Ni. Similar behavior has been observed in $Ca(Fe_{0.1}Co_{0.9})_2P_2$ and $Ca(Fe_{1-x}Ni_x)_2P_2$ ($x = 0.5$ and 0.6).³² In order to obtain the electronic specific heat and Debye temperature, we fit the $C_p/T - T^2$ curve between 5 and 10 K by using the formula $C_p/T = \gamma + \beta_3 T^2 + \beta_5 T^4$. We obtain $\gamma = 48(2) \text{ mJ mol}^{-1} \text{ K}^{-2}$, $\beta_3 = 1.06(8) \text{ mJ mol}^{-1} \text{ K}^{-4}$, and $\beta_5 = 5.4(6) \mu\text{J mol}^{-1} \text{ K}^{-6}$. The Debye temperature is estimated to be $\Theta_D = 209(5) \text{ K}$ using the formula $\Theta_D = (12\pi^4 NR/5\beta)^{1/3}$, where N is the atomic number in the chemical formula ($N = 5$) and R is the gas constant ($R = 8.314 \text{ J mol}^{-1} \text{ K}^{-1}$). The Debye temperature

Θ_D and electronic specific heat γ are close to the results obtained on the KNi_2Se_2 polycrystals.¹⁹ The large γ implies the mass enhancement at low temperatures and heavy-fermion-like behavior.¹⁹ Moreover, the Θ_D is also similar to that of $\text{K}_x\text{Fe}_{2-y}\text{Se}_2$ (~ 212 K),³³ which could be ascribed to the similar structure and atomic weight. As shown in the inset of Fig. 6, at high temperature heat capacity approaches the Dulong-Petit value of 3NR ($124.71 \text{ J mol}^{-1} \text{ K}^{-1}$).

From obtained A and γ , the Kadowaki-Woods (KW) ratio $A/\gamma^2 = 3.43(6) \times 10^{-6} \mu\Omega \text{ cm mol}^2 \text{ K}^2 \text{ mJ}^{-2}$. This is somewhat smaller than value for KNi_2Se_2 polycrystals ($1.2 \times 10^{-5} \mu\Omega \text{ cm mol}^2 \text{ K}^2 \text{ mJ}^{-2}$),¹⁹ and from the universal value observed in strongly correlated heavy fermion systems ($1 \times 10^{-5} \mu\Omega \text{ cm mol}^2 \text{ K}^2 \text{ mJ}^{-2}$).³⁴ However, it is still larger than that in many intermediate valence Yb-based and several Ce-based compounds with large γ ($A/\gamma^2 \sim 0.4 \times 10^{-6} \mu\Omega \text{ cm mol}^2 \text{ K}^2 \text{ mJ}^{-2}$).³⁴ On the other hand, from fitted temperature-independent susceptibility χ_0 ($1.87(5) \times 10^{-3}$ and $4.69(4) \times 10^{-3}$ emu mol f.u.⁻¹ Oe⁻¹ for H||ab and H||c) and the relation of $\chi_{\text{Landau}} \approx -1/3\chi_{\text{Pauli}}$ when ignoring the core and orbital diamagnetism, $\chi_{\text{Pauli}} \approx 2.81 \times 10^{-3}$ and 7.04×10^{-3} emu mol f.u.⁻¹ Oe⁻¹ for H||ab and H||c. The estimate of the Wilson's ratio ($R_W = \frac{\pi^2 k_B^2}{3\mu_B^2} \frac{\chi_{\text{Pauli}}}{\gamma}$) gives large values $R_W = 4.26$ and 10.68 for H||ab and H||c, which is much larger than that in a noninteracting Fermi liquid, where R_W is expected to be close to 1. This value is also larger than derived from polycrystalline ($R_W = 1.7$).¹⁹ Such large values have been found in the heavy Fermi liquids ($R_W = 1 - 6$).³⁵ Large R_W values also occur in the system

with a magnetic instability or strong exchange enhanced paramagnetic state.³⁶ All this implies heavy fermion-like ground state in KNi_2Se_2 crystals at low temperature.

IV. CONCLUSION

In summary, we synthesized $\text{K}_{0.95}\text{Ni}_{1.86}\text{Se}_2$ single crystals using self-flux method. Different from polycrystals, there are small K and Ni deficiencies, similar to iron based counterpart $\text{K}_x\text{Fe}_{2-y}\text{Se}_2$. Resistivity measurement indicates that the $\text{K}_{0.95}\text{Ni}_{1.86}\text{Se}_2$ single crystal does not exhibit a superconducting transition down to 0.3 K, in contrast to polycrystals. Therefore, superconducting state is rather sensitive to K and Ni stoichiometry similar to KFe_2Se_2 . Our results suggest a Fermi surface reconstruction below 30 K, corresponding to the transition from local CDW state to heavy fermion state at low temperature.

V. ACKNOWLEDGEMENT

Work at Brookhaven is supported by the U.S. DOE under Contract No. DE-AC02-98CH10886 and in part by the Center for Emergent Superconductivity, an Energy Frontier Research Center funded by the U.S. DOE, Office for Basic Energy Science (H. L. and C. P). Work at the National High Magnetic Field Laboratory is supported by the DOE NNSA DEFG52-10NA29659 (D.G.), by the NSF Cooperative Agreement No. DMR-0654118, and by the state of Florida.

-
- ¹ Y. Kamihara, T. Watanabe, M. Hirano, and H. Hosono, *J. Am. Chem. Soc.* **130**, 3296 (2008).
- ² T. Watanabe, H. Yanagi, T. Kamiya, Y. Kamihara, H. Hiramatsu, M. Hirano, H. Hosono, *Inorg. Chem.* **46** 7719 (2007).
- ³ T. Watanabe, H. Yanagi, Y. Kamihara, T. Kamiya, M. Hirano, H. Hosono, *J. Solid State Chem.* **181** 2117 (2008).
- ⁴ V. L. Kozhevnikov, O. N. Leonidova, A. L. Ivanovskii, I. R. Shein, B. N. Goshchitskii, and A. E. Karkin, *JETP Lett.* **87** 649 (2008).
- ⁵ T. Mine, H. Yanagi, T. Kamiya, Y. Kamihara, M. Hirano and Hideo Hosono, *Solid State Comm.* **147** 111 (2008).
- ⁶ F. Ronning, E. D. Bauer, T. Park, S.-H. Baek, H. Sakai, and J. D. Thompson, *Phys. Rev. B* **79** 134507 (2009).
- ⁷ F. Ronning, E. D. Bauer, T. Park, N. Kurita, T. Klimczuk, R. Movshovich, A. S. Sefat, D. Mandrus, J. D. Thompson, *Physica C* **469**, 396 (2009).
- ⁸ F. C. Hsu, J. Y. Luo, K. W. Yeh, T. K. Chen, T. W. Huang, P. M. Wu, Y. C. Lee, Y. L. Huang, Y. Y. Chu, D. C. Yan, and M. K. Wu, *Proc. Natl. Acad. Sci. USA* **105**, 14262 (2008).
- ⁹ K.-W. Yeh, T. W. Huang, Y. L. Huang, T. K. Chen, F. C. Hsu, P. M. Wu, Y. C. Lee, Y. Y. Chu, C. L. Chen, J. Y. Luo, D. C. Yan, and M. K. Wu, *EPL* **84**, 37002 (2008).
- ¹⁰ Y. Mizuguchi, F. Tomioka, S. Tsuda, T. Yamaguchi, and Y. Takano, *Appl. Phys. Lett.* **94**, 012503 (2009).
- ¹¹ J. Guo, S. Jin, G. Wang, S. Wang, K. Zhu, T. Zhou, M. He, and X. Chen, *Phys. Rev. B* **82**, 180520(R) (2010).
- ¹² A. F. Wang, J. J. Ying, Y. J. Yan, R. H. Liu, X. G. Luo, Z. Y. Li, X. F. Wang, M. Zhang, G. J. Ye, P. Cheng, Z. J. Xiang, and X. H. Chen, *Phys. Rev. B* **83**, 060512 (2011).
- ¹³ C.-H. Li, B. Shen, F. Han, X. Y. Zhu, and H.-H. Wen, *Phys. Rev. B* **83**, 184521 (2011).
- ¹⁴ R. H. Liu, X. G. Luo, M. Zhang, A. F. Wang, J. J. Ying, X. F. Wang, Y. J. Yan, Z. J. Xiang, P. Cheng, G. J. Ye, Z. Y. Li and X. H. Chen, *Europhys. Lett.* **94**, 27008 (2011).
- ¹⁵ A. Krzton-Maziopa, Z. Shermadini, E. Pomjakushina, V. Pomjakushin, M. Bendele, A. Amato, R. Khasanov, H. Luetkens, and K. Conder, *J. Phys.: Condens. Matter* **23**, 052203 (2011).
- ¹⁶ M. H. Fang, H. D. Wang, C. H. Dong, Z. J. Li, C. M. Feng, J. Chen, H. Q. Yuan, *EPL* **94**, 27009 (2011).
- ¹⁷ N. Umeyama, M. Tokumoto, S. Yagi, M. Tomura, K. Tokiwa, T. Fujii, R. Toda, N. Miyakawa, and S.-I. Ikeda, *Jpn. J. Appl. Phys.* **51**, 053001 (2012).
- ¹⁸ A. R. Newmark, G. Huan, and M. Greenblatt, and M. Croft, *Solid State Commun.*, **71** 1025 (1989).

- ¹⁹ J. R. Neilson, A. Llobet, A. V. Stier, L. Wu, J. Wen, J. Tao, Y. Zhu, Z. B. Tesanovic, N. P. Armitage, and T. M. McQueen, *Phys. Rev. B* **86**, 054512 (2012).
- ²⁰ H. C. Lei and C. Petrovic, *Phys. Rev. B* **83**, 184504 (2011).
- ²¹ B. Hunter, "Rietica - A visual Rietveld program", International Union of Crystallography Commission on Powder Diffraction Newsletter No. **20**, (Summer) <http://www.rietica.org> (1998).
- ²² J. R. Neilson and T. M. McQueen, *J. Am. Chem. Soc.* **134**, 7750 (2012).
- ²³ J. G. Speight, *Lange's Handbook of Chemistry*, 16th ed. (Mc Graw-Hill, London, 2005), p. 1.153.
- ²⁴ C. Cao, J.-H. Dai, *Chin Phys. Lett.* **28**, 057402 (2011).
- ²⁵ A. C. Ehrlich and D. Rivier, *J. Phys. Chem. Solids.* **29**, 1293 (1968).
- ²⁶ R. L. Carlin, *Magnetochemistry* (Springer, New York, 1986).
- ²⁷ Z. P. Yin, K. Haule, and G. Kotliar, *Nat. Mater.* **10**, 932 (2011).
- ²⁸ H. Yang, Y. Liu, C. G. Zhuang, J. R. Shi, Y. G. Yao, S. Massidda, M. Monni, Y. Jia, X. X. Xi, Q. Li, Z. K. Liu, Q. R. Feng, and H. H. Wen, *Phys. Rev. Lett.* **101**, 067001 (2008).
- ²⁹ P. Cheng, H. Yang, Y. Jia, L. Fang, X. Zhu, G. Mu, and H.-H. Wen, *Phys. Rev. B* **78**, 134508 (2008).
- ³⁰ A. S. Sefat, M. A. McGuire, B. C. Sales, R. Jin, J. Y. Howe, and D. Mandrus, *Phys. Rev. B* **77**, 174503 (2008).
- ³¹ R. A. Smith, *Semiconductors* (Cambridge University Press, Cambridge, 1978).
- ³² S. Jia, S. Chi, J. W. Lynn, and R. J. Cava, *Phys. Rev. B* **81**, 214446 (2010).
- ³³ B. Zeng, B. Shen, G. F. Chen, J. B. He, D. M. Wang, C. H. Li, and H. H. Wen, *Phys. Rev. B* **83**, 144511 (2011).
- ³⁴ N. Tsujii, K. Yoshimura, and K. Kosuge, *J. Phys.: Condens. Matter* **15**, 1993 (2003).
- ³⁵ L. E. DeLong, R.P. Guertin, S. Hasanain, and T. Fariss, *Phys. Rev. B* **31**, 7059 (1985).
- ³⁶ S. R. Julian, A. P. Mackenzie, G. G. Lonzarich, C. Berge-
mann, R. K. W. Haselwimmer, Y. Maeno, S. NishiZaki,
A. W. Tyler, S. Ikeda, and T. Fujita, *Physica B* **259-261**,
928 (1999).